Computational Biology and Chemistry 123 (2026) 108997

Contents lists available at ScienceDirect

Computational Biology and Chemistry

journal homepage: www.elsevier.com/locate/cbac

Hydrogen bonding and membrane anchoring of the antimicrobial peptide NP-3a investigated through molecular dynamics

Ana Clara D. Aquino, Karinna Mendanha, Herbert de C. Georg, Guilherme Colherinhas *

Instituto de Física, Universidade Federal de Goiás, Goiânia, GO 74690-900, Brazil

ARTICLE INFO

Keywords:
Antimicrobial peptides
NP-3a
Molecular dynamics simulation
DOPC bilayer
Hydrogen bonding

ABSTRACT

Antimicrobial peptides (AMPs) are emerging as critical alternatives to antibiotics in the fight against multidrug resistance. NP-3a, a rabbit defensin, combines structural stability with broad-spectrum activity, yet its molecular mechanism of membrane interaction remains unclear. Here, we employed atomistic molecular dynamics simulations to investigate NP-3a in vacuum, aqueous solution, and at a DOPC lipid bilayer interface. In solution, NP-3a shifted from a compact β-sheet stabilized by ~23 intramolecular HBs to a dynamic state engaging extensively with water (~122 HBs, lifetime ~9.6 ps). At the membrane interface, NP-3a achieved stable anchoring with ~39% insertion, mediated by ~12 long-lived hydrogen bonds (~2.9 ns lifetime) with DOPC headgroups and a binding free energy of 24.3 kJ/mol. Residue-level analysis revealed Arg-7 to Arg-9 as dominant contributors through electrostatic anchoring to phosphate groups, reinforced by serine- and cysteine-mediated contacts. Notably, NP-3a remained localized at the membrane surface without penetrating the hydrophobic core, supporting a selective surface-associated mechanism of action. These findings provide atomistic insights into NP-3a's interaction with eukaryotic-like membranes and highlight molecular determinants relevant for the rational design of next-generation AMPs.

1. Introduction

Infectious diseases remain one of the major global challenges to public health, largely due to the increasing prevalence of antimicrobial resistance (AMR). It is estimated that by 2050, the annual number of deaths related to AMR could reach 10 million worldwide (Osei et al., 2025). In this context, antimicrobial peptides (AMPs), components of innate immunity across plants, animals, and microorganisms, are emerging as promising alternatives to conventional antibiotics (Huan et al., 2020). Their functional versatility, rapid action, and low propensity for the development of resistance have made them a growing focus of research and development (Yang et al., 2025).

AMPs exhibit multifaceted mechanisms of action, being able to interact directly with bacterial membranes through electrostatic and hydrophobic forces, leading to pore formation, cell lysis, or bilayer destabilization (Huan et al., 2020). In addition, some peptides can modulate the host immune system, adding anti-inflammatory and immunoregulatory properties to their antimicrobial activity (Aunpad and Thitirungreangchai, 2025). These features distinguish AMPs from classical antibiotics, which typically act on a single enzymatic or structural target (Luo et al., 2023). Several recent studies have demonstrated that the structural self-assembly of AMPs can enhance their antimicrobial efficacy. For example, the formation of nanofibers by chimeric or self-assembling peptides contributes to increased physiological stability and efficient bacterial capture (Ma et al., 2025; Yuan et al., 2025). Supramolecular structures such as micelles, nanotubes, and nanofibers are also advantageous because they locally concentrate peptides, thereby enhancing their interaction with bacterial membranes (Yu et al., 2024; Du et al., 2022). This capacity to form hierarchical arrangements in biological environments broadens the therapeutic potential of AMPs.

Another central point in the development of novel AMPs is the pursuit of chemical strategies that improve their stability and selectivity. Approaches such as conjugation to conventional antibiotics, hydrocarbon stapling, and N-glycosylation of arginine residues have already been tested successfully, leading to derivatives that are more resistant to proteolysis, exhibit greater helicity, and show reduced hemolysis (Peng et al., 2025; Li et al., 2025). These modifications, in addition to expanding the therapeutic window, preserve or even enhance the mechanism of action based on membrane lysis, highlighting the

* Corresponding author.
E-mail address: gcolherinhas@ufg.br (G. Colherinhas).

https://doi.org/10.1016/j.compbiolchem.2026.108997
Received 13 January 2026; Received in revised form 19 February 2026; Accepted 28 February 2026
Available online 2 March 2026

importance of structural and dynamic studies that explore such interactions. Over the past years, the literature has also reported significant efforts to characterize how AMPs interact with different lipid compositions. A study on rabbit defensins demonstrated that bilayer composition determines not only the intensity but also the pattern of permeabilization: vesicles containing PE, PG, and cardiolipin presented large transient lesions, whereas systems composed of pure POPG exhibited slow and gradual leakage (Hristova et al., 1997). Although antimicrobial peptides primarily target bacterial membranes enriched in anionic lipids such as phosphatidylglycerol and cardiolipin, *zwitterionic* lipid bilayers composed of phosphatidylcholine provide an important reference model to probe peptide selectivity. DOPC membranes are widely used as simplified eukaryotic-like systems to evaluate whether AMPs exhibit strong surface adsorption or deep insertion in the absence of net membrane charge. In this context, DOPC serves as a controlled model to assess the propensity of NP-3a to interact with *zwitterionic* membranes, which is directly related to antimicrobial selectivity and reduced cytotoxicity toward host cells.

The therapeutic potential of AMPs has also been validated in in vivo experimental models. Peptides such as FWK have shown efficacy against multidrug-resistant Klebsiella pneumoniae, with promising results in murine tests (Liu et al., 2025). Innovative conjugates, such as paenipeptins linked to ciprofloxacin, demonstrated dual action (membrane disruption and intracellular inhibition of DNA gyrase) while also accelerating wound healing in infected tissues (Peng et al., 2025). These findings indicate that AMPs may act in a multifunctional manner, combining direct antimicrobial activity with additional benefits for the host. Beyond therapeutic applications, the structural and functional diversity of AMPs has fueled interest in understanding their mechanisms of action at the molecular level. Studies on supramolecular self-assembly, acid-induced resistance, and specific interactions with lipopolysaccharides (LPS) reveal that small changes in sequence or environment can result in substantial alterations in antimicrobial performance (Hwang and Kim, 2024; Castelletto et al., 2024, 2018; Edwards-Gayle and Hamley, 2017; Schmidtchen and Malmsten, 2013). Therefore, systematic investigation of these properties through theoretical and computational approaches complements experimental work, enabling the elucidation of phenomena that are difficult to capture exclusively in laboratory settings.

Although rabbit defensins have been biochemically characterized, the molecular determinants governing their selective surface binding versus membrane insertion remain poorly resolved. In particular, the atomistic basis for NP-3a's interfacial stabilization (despite strong cationic charge and broad antimicrobial activity) has not been elucidated. Understanding why NP-3a anchors rather than penetrates *zwitterionic* bilayers is essential to explain its selectivity toward bacterial membranes and to guide rational AMP engineering. Within this context, the present study focuses on the antimicrobial peptide NP-3a, a member of the rabbit defensin family. NP-3a contains 33 amino acid residues and exhibits a characteristic defensin fold, stabilized by three disulfide bridges that reinforce its β-structure and confer remarkable structural stability (Hristova et al., 1997). Its primary sequence has been identified as GICACRRRFCPNSERFSGYCRVNGARYVRCCSRR (Huan et al., 2020), and classical studies have demonstrated its activity against Gram-positive and Gram-negative bacteria, as well as antiviral and antifungal properties (Huan et al., 16, 2020). NP-3a belongs to the group of defensins NP-1 through NP-5, of which NP-1, NP-2, NP-3a, and NP-3b are highly active in permeabilizing lipid vesicles derived from E. coli, in contrast to NP-4 and NP-5, which display low activity when tested individually (Hristova et al., 1997). Experimental evidence suggests that specific cationic residues, such as Arg or Lys, play a crucial role in the interaction with negatively charged lipids, thereby modulating permeabilization (Hristova et al., 1997). In this study, we employ atomistic molecular dynamics simulations to investigate the interfacial behavior of NP-3a in aqueous solution and in contact with a DOPC lipid bilayer. The primary objective is to elucidate the physicochemical determinants that govern surface anchoring versus membrane insertion, with quantitative characterization of interaction energies, hydrogen bond (HBs) networks, and structural adaptation at the lipid-water interface. Here, surface anchoring is defined as the persistent localization of the peptide at the lipid headgroup region, stabilized by electrostatic and HBs interactions without penetration into the hydrophobic core of the bilayer. In contrast, membrane insertion refers to deep penetration of the peptide beyond the interfacial headgroup region into the hydrophobic interior of the membrane. The DOPC bilayer was deliberately selected as a *zwitterionic*, eukaryotic-like reference system that allows evaluation of peptide selectivity in the absence of net membrane charge and enables direct comparison with previous defensin studies. Thus, the purpose of this work is not to explore membrane compositional diversity, but to establish a controlled mechanistic framework for understanding how NP-3a stabilizes at neutral membrane interfaces. We hypothesize that NP-3a preferentially adopts a persistent interfacial anchoring state mediated by arginine-driven electrostatic recognition and cysteine-stabilized structural locking, rather than deep penetration into *zwitterionic* bilayers. To test this hypothesis, we adopt a hierarchical simulation strategy contrasting vacuum, aqueous, and membrane-associated environments, thereby disentangling intrinsic peptide properties from solvent- and membrane-induced effects.

2. Methodology

The NP-3a peptide belongs to the family of rabbit neutrophil defensins (NP-1 to NP-5), a class of antimicrobial peptides characterized by a high density of cationic residues and multiple cysteines arranged in intramolecular disulfide bonds. NP-3a consists of 33 amino acids, with its primary sequence identified as GICACRRRFCPNSERFSGYCRVNGARYVRCCSRR (Huan et al., 16, 2020). The sequence is notably enriched in arginine (Arg) and cysteine (Cys) residues, the latter being essential for the formation of three disulfide bridges, which stabilize the β-sheet conformation typical of defensins (Hristova et al., 1997). Structurally, NP-3a adopts a predominantly β-sheet fold, stabilized not only by disulfide bonds but also by a hydrophobic core that restricts conformational flexibility. This architecture confers the peptide with high thermal stability and resistance to proteolytic degradation, properties that have been reported in comparative studies with other members of the same family (Hristova et al., 1997). Moreover, the amphipathic profile of NP-3a, arising from the spatial distribution of hydrophobic and positively charged regions, allows it to selectively interact with biological membranes, particularly those enriched in anionic lipids such as phosphatidylglycerol (PG) and cardiolipin (Hristova et al., 1997).

Functionally, NP-3a displays broad-spectrum antimicrobial activity, including action against Gram-positive and Gram-negative bacteria, fungi, and even antiviral effects (Huan et al., 2020). Its effectiveness has been demonstrated in model vesicle assays: NP-1, NP-2, NP-3a, and NP-3b induce marked permeabilization of liposomes derived from Escherichia coli, whereas NP-4 and NP-5 were inactive when tested individually (Hristova et al., 1997). These findings highlight the importance of specific basic residues (such as Arg21 and Lys21 in peptide primary sequence) in mediating electrostatic interactions with lipid phosphate groups, suggesting that even subtle sequence variations can drastically affect antimicrobial performance (Hristova et al., 1997). NP-3a represents an ideal model for computational investigations, as it combines well-characterized structural properties, a short and biologically relevant sequence, and experimentally supported mechanisms of membrane interaction. In the present study, NP-3a will serve as the starting point for molecular dynamics simulations performed in aqueous solution and in contact with a DOPC lipid bilayer, with the aim of exploring in greater detail the molecular determinants that govern its anchoring and the HBs interactions established with the polar headgroups of the lipids. Fig. 1 shows the NP-3a peptide and its primary sequence.

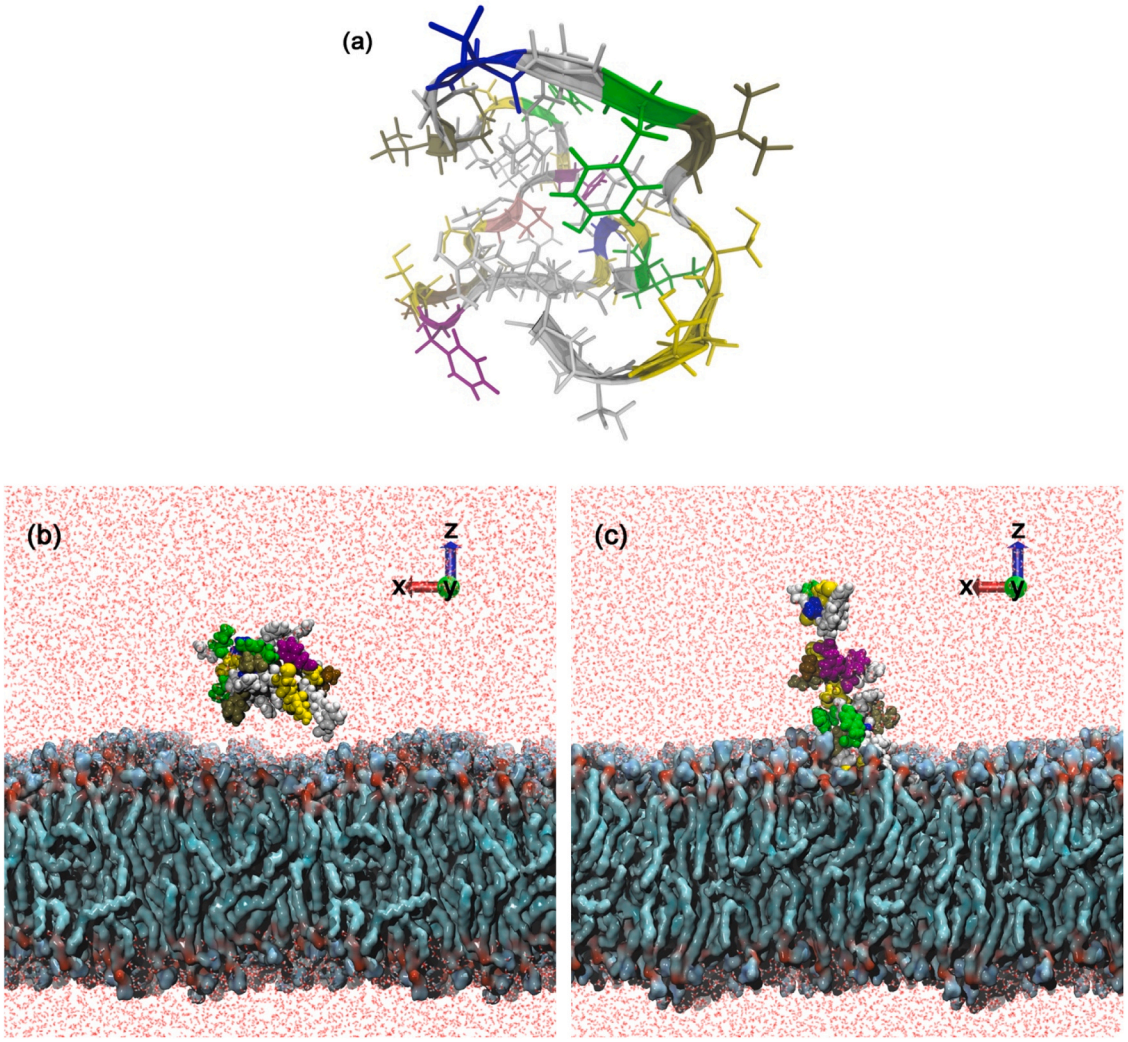

Fig. 1. (a) Representation of the NP-3a peptide and its primary sequence: GICACRRRFCPNSERFSGYCRVNGARYVRCCSRR; and on the DOPC membrane (b) initial and (c) final configuration.

The initial structure of the NP-3a peptide was constructed using the PyMOL molecular graphics program (Schrödinger, 2015), based exclusively on the primary amino acid sequence reported in Ref (Huan et al., 2020). No experimentally resolved three-dimensional structure was used as initial input for molecular dynamics simulations. The peptide was manually built in PyMOL from its sequence, and the resulting conformation served only as an initial starting geometry for the MD-simulations. Although the initial geometry was constructed using PyMOL, this structure served only as a starting configuration derived from the primary sequence. All secondary and tertiary structural features emerged from energy minimization and equilibration under the CHARMM36 all-atom force field (Brooks et al., 2009; Best et al., 2012). Therefore, the final conformational ensemble reflects thermodynamic relaxation under the selected simulation conditions rather than the arbitrary features of the initial model. All structural features (including secondary organization and intramolecular interactions) emerged during energy minimization and equilibration under the selected force field, ensuring that the final conformational ensemble was not biased by the initial geometry. The peptide water-converged structure was placed in proximity to a pre-assembled 1,2-dioleoyl-sn-glycero-3-phosphocholine (DOPC) lipid bilayer (Alves et al., 2020). A parallel system was also constructed in which NP-3a was solvated in water without lipids, enabling comparative analyses in the absence of a membrane. In both cases, explicit TIP3P water molecules were used as solvent (Jorgensen et al., 1996, 1983).

All molecular dynamics simulations were carried out using the CHARMM36 all-atom force field (Brooks et al., 2009; Best et al., 2012), which provides residue-specific parametrization and explicitly describes all bonded and non-bonded interactions at the atomic level. CHARMM36 is among the most extensively validated and widely accepted force fields for peptide and protein simulations (Oliveira and Colherinhas, 2020; Colherinhas, 2021a, 2021b), making it particularly suitable for investigating conformational adaptation and environment-dependent stabilization of antimicrobial peptides. The peptide topology is constructed by grouping individually parameterized residues into a single molecular entity, following standard procedures in atomistic molecular dynamics. No artificial constraints or predefined interaction locks were imposed during the simulations. Instead, all intramolecular and intermolecular interactions were allowed to evolve freely according to the force field parameters and the simulation conditions. This unconstrained approach ensures that the structural and dynamical properties of NP-3a emerge naturally from the balance of electrostatic, van der Waals, and HBs interactions, without bias toward any predefined structural arrangement. All simulations were performed with GROMACS (Abraham et al., 2023, 2015).

Long-range electrostatics were computed using the Particle Mesh Ewald (PME) method (Darden et al., 1993) with a real-space cutoff of 1.2 nm, while van der Waals interactions employed the same cutoff

distance. Bond constraints involving hydrogen atoms were treated with the LINCS algorithm (Hess et al., 1997), enabling the use of a 1 fs integration time step. The temperature was maintained at 300 K using the velocity rescaling thermostat (Bussi et al., 2007), and the pressure was controlled at 1 atm employing the Parrinello-Rahman barostat (Parrinello and Rahman, 1981). All simulations were performed under alternating NVT and NPT ensembles, with semi-isotropic pressure coupling applied to the lipid bilayer during NPT conditions. The equilibration protocol consisted (also performed in previous studies (Alves et al., 2020; Coelho et al., 2023; Malaspina et al., 2017; Mendanha and Colherinhas, 2024) of an initial 50 ns equilibration stage, followed by three consecutive production runs of 50 ns, 50 ns, and 100 ns, resulting in a total simulation time of 200 ns. This timescale was not intended to capture rare events such as full membrane penetration or translocation, which are known to occur on microsecond timescales and typically require enhanced sampling approaches. Instead, the simulation strategy was designed to characterize stable interfacial states of NP-3a at the membrane surface.

To accelerate access to relevant peptide-membrane configurations within a feasible computational timeframe, NP-3a was initially positioned in close proximity to the DOPC bilayer. This setup allows the system to rapidly explore surface-recognition and anchoring regimes, which are the primary focus of the present study. Stable peptide anchoring at the membrane interface was established during the early stages of the production runs and remained consistent throughout the remainder of the simulations. To ensure statistical robustness, only the final 100 ns of the production trajectory (during which the peptide remained persistently anchored-were used for quantitative analyses). Configurations were sampled uniformly from this equilibrated segment, corresponding to 50% of the total production frames, thereby ensuring that all reported structural and energetic properties reflect a converged interfacial state. This setup allowed systematic investigation of peptide behavior both in aqueous solution and in a membrane-bound state, providing the basis for detailed analysis of interaction energies, anchoring stability, and the HBs network between NP-3a and the DOPC polar headgroups. Chloride ions were added using Packmol software to neutralize the total charge in all simulated system, since NP-3a carries a net charge of $+8e$. The DOPC bilayer was pre-equilibrated in pure water for approximately 300 ns prior to the introduction of the NP-3a peptide. Table 1 shows the composition for all simulated systems: System A: NP-3a in water; and System B: NP-3a and DOPC in water. For visualization we use VMD program (Humphrey et al., 1996).

The simulation protocol adopted in this work follows a hierarchical and comparative strategy designed to disentangle intrinsic peptide properties from environmentally induced effects. Simulations in vacuum were not intended to mimic physiological conditions, but rather to provide a reference state in which NP-3a structural stabilization arises exclusively from intramolecular interactions, such as disulfide bridges, electrostatics, and HBs. This reference allows quantification of the maximal compaction and internal energetic contributions of the peptide in the absence of dielectric screening. Subsequent simulations in aqueous solution and at the DOPC-water interface progressively introduce solvent and membrane effects, enabling a systematic assessment of how hydration and lipid interactions modulate peptide structure, dynamics, and anchoring. Such a stepwise approach is commonly employed in molecular dynamics studies of antimicrobial peptides to rationalize environmental contributions to membrane recognition and selectivity

Trajectory analyses were performed using the standard tools available within the GROMACS package (Abraham et al., 2023, 2015), complemented with in-house scripts for statistical treatment. To quantify peptide-lipid interactions, we computed interaction energies between NP-3a and the DOPC bilayer, separating the Coulombic and van der Waals contributions. Throughout the analyzed production stage, the peptide remained stably associated with the membrane interface, and no binding-unbinding events were sampled. Consequently, membrane-binding behavior was characterized through time-averaged interaction energies and structural descriptors computed over the equilibrated trajectory segment, reflecting stabilized interfacial states rather than kinetic binding transitions. Particular attention was given to the HBs network between NP-3a and the lipid headgroups. HBs were defined using the standard GROMACS criteria: a donor-acceptor distance ≤ 0.35 nm and a hydrogen-donor-acceptor angle $\leq 30°$. The average number of HBs, their lifetimes (Luzar, 2000; Luzar and Chandler, 1996; Van Der Spoel et al., 2006), and the distribution of donor/-acceptor pairs were calculated across the production trajectories, enabling assessment of anchoring stability. The corresponding free energy of HBs rupture (ΔG) was estimated from HBs population and kinetic correlation analysis [38–40]. In addition, mass density profiles along the bilayer normal (z-axis) were also extracted to characterize the depth of insertion of NP-3a into the lipid bilayer. For comparative purposes, simulations of NP-3a in aqueous solution without lipids were analyzed for solvent-accessible surface area (SASA); Einstein's Diffusion Coefficient (Mean Square Displacement, MSD) and intramolecular HBs, in order to contrast conformational dynamics in the absence of membrane anchoring. All statistical analyses were performed over the 50% of stored configurations from the production runs, ensuring robust sampling. Reported averages were obtained after discarding the equilibration phase, and uncertainties were quantified as the standard error of the mean across the last independent production blocks (100 ns). It is important to note that defensin folds are environment-dependent. Structural adaptation in vacuum, aqueous solution, or at membrane interfaces may differ due to dielectric screening and lipid interactions. Therefore, direct comparison with experimentally resolved homologous defensins under distinct conditions should be interpreted cautiously.

Table 1
Composition of the simulation boxes containing a single NP-3a molecule in aqueous solution (System A) and a single NP-3a molecule in aqueous solution in the presence of a DOPC lipid bilayer (System B). In both systems, chloride ions were added to neutralize the total charge, since NP-3a carries a net atomic charge of + 8e.

Molecules	*# Atoms*	*System A*	*System B*
NP-3a	549	1	1
DOPCs	138	–	128
Ions (Cl^-)	1	8	8
Water	3	4104	23,275
Total Atoms	—	12,869	88,046

Table 2
Coulomb (E_C) and Lennard-Jones (E_{LJ}) interaction energies for the components of Systems A and B. Values are reported in kJ/mol. Results obtained for the peptide in vacuum were also included for comparison. Here, peptide-peptide interaction refers to intramolecular interactions within the single NP-3a molecule.

	E_{LJ}		
	In vacuum	**In water**	**In DOPC-water**
Peptide-Peptide	-740.5 ± 33.4	-533.9 ± 45.0	-624.8 ± 67.6
Peptide-Ions	236.7 ± 34.6	4.3 ± 11.3	1.4 ± 7.1
Peptide-Water	–	-774.6 ± 71.2	-533.9 ± 90.3
Peptide-DOPC	–	–	-272.7 ± 42 5
	E_C		
	In vacuum	**In water**	**In DOPC-water**
Peptide-Peptide	-2779.7 ± 92.7	-2334.3 ± 115.5	-2274.7 ± 134.0
Peptide-Ions	-2743.8 ± 73.6	-131.0 ± 112.2	-51.7 ± 75.6
Peptide-Water	–	-4394.4 ± 195.1	-3661.4 ± 280.2
Peptide-DOPC	–	–	-842.0 ± 152.7

3. Results and discussion

3.1. Energy interaction

The peptide-peptide (intramolecular interactions within the single NP-3a molecule) Coulomb interaction in vacuum was −2779.7 kJ/mol (see Table 2). When solvated in water, this interaction decreased in magnitude to −2334.3 kJ/mol, corresponding to a 16% reduction relative to vacuum. This attenuation reflects the strong dielectric screening of water, which diminishes direct electrostatic attraction/repulsion between charged residues of NP-3a. Upon insertion into the DOPC-water system, the peptide-peptide Coulomb interaction further decreased slightly to −2274.7 kJ/mol, an overall 18% reduction compared to vacuum. The stabilization provided by hydration shells and ion–lipid competition thus significantly weakens intrapeptide electrostatics. This trend reflects the progressive reduction of Coulomb interactions as environmental polarity increases. In water, screening is dominated by solvent molecules, whereas in the bilayer system, additional stabilization arises from competition with negatively charged lipid headgroups and chloride ions. The data suggest that NP-3a's electrostatic intramolecular network is flexible and environment-dependent, with strong interactions in vacuum that are progressively compensated in aqueous and membrane environments. For peptide–peptide Lennard-Jones (van der Waals) interactions, the energy in vacuum was −740.5 kJ/mol. When the peptide was solvated in water, this value decreased to −533.9 kJ/mol, representing a 28% reduction compared to vacuum.

In the DOPC-water system, the peptide-peptide E_{LJ} interaction became slightly stronger again (−624.8 kJ/mol), representing a 16% increase relative to the aqueous system, although still 15.6% weaker than in vacuum. This trend reflects the balance between environmental screening and interfacial stabilization. In vacuum, the absence of solvent maximizes intramolecular van der Waals contacts. Upon solvation, these contacts are partially reduced due to competition with solvent interactions. In the presence of the lipid bilayer, partial recovery of E_{LJ} interactions suggests a moderate increase in peptide compactness and favorable interfacial packing, rather than structural collapse. Thus, Lennard-Jones contributions reflect the balance between peptide self-association forces and external stabilization by solvent or membrane. The increase in E_{LJ} strength from water to DOPC-water suggests that NP-3a regains some compactness or engages in favorable hydrophobic contacts in the presence of the bilayer. When comparing the two contributions, Coulombic interactions dominate by at least one order of magnitude across all environments. For instance, in water the peptide-peptide E_C (−2334.3 kJ/mol) is more than 4.3 times stronger than the corresponding E_{LJ} (−533.9 kJ/mol). In DOPC-water, this ratio is reduced to 3.6, reflecting the fact that van der Waals interactions gain relative importance at the membrane interface. In vacuum, Coulomb interactions are still stronger by a factor of 3.8, highlighting the intrinsic dominance of electrostatics in NP-3a stabilization. Quantitatively, the transition from vacuum to water leads to a 16% reduction in E_C but a much larger 28% reduction in E_{LJ}, indicating that peptide compactness is more strongly affected by solvation than electrostatics. The insertion into the membrane restores ~16% of E_{LJ} interactions but only ~2.5% of E_C, suggesting that hydrophobic contacts are preferentially re-established at the lipid interface, whereas electrostatics remain largely screened.

The peptide-DOPC Coulomb interaction in the membrane system was measured at −842 kJ/mol, highlighting the strong electrostatic attraction between NP-3a and the negatively charged phosphate groups of DOPC headgroups. This contribution is substantial, though weaker than peptide–water interactions (−3661.4 kJ/mol), reflecting the fact that only a subset of residues, particularly cationic side chains such as arginine and lysine, directly interact with the lipid interface. Nevertheless, this energy is more than three times stronger than the peptide-ion Coulomb interaction (−51.7 kJ/mol), confirming that lipids, rather than counterions, act as the primary partners in stabilizing NP-3a anchoring at the bilayer surface. In addition to electrostatics, Lennard-Jones interactions between NP-3a and DOPC contribute −272.7 kJ/mol, which, although smaller in magnitude, provides essential stabilization through van der Waals contacts. These interactions suggest partial insertion of hydrophobic or amphipathic residues into the interfacial region of the bilayer, consistent with the observed ~39% penetration of the peptide. Together, Coulomb and van der Waals contributions indicate a synergistic anchoring mechanism, where electrostatics drive recognition of lipid headgroups and van der Waals forces fine-tune the stabilization of NP-3a at the interface without promoting deep penetration into the hydrophobic core.

3.2. Statistical and energetic signatures of hydrogen bonding

A global analysis of HBs highlights a marked dependence on the simulated environment. In vacuum, NP-3a exhibited an average of ~23 (± 2) intramolecular HBs (see Table 3), reflecting the strong compaction tendency in this medium. Upon solvation in water, this number dropped to ~6 (± 2) HBs, corresponding to a ~74% reduction, demonstrating disruption of the internal HBs network in favor of interactions with water molecules. In the presence of the DOPC bilayer, the number of intramolecular HBs increased to ~4 (± 2), representing a ~33% decrease compared to the aqueous environment, indicating that the spatial restriction imposed by the membrane. Moreover, intermolecular interactions became dominant in hydrated environments: in solution, the peptide formed on average ~122 (± 6) HBs with solvent, a number that decreased to ~110 (± 7), −10%, in the presence of DOPC, while in parallel, 12 (± 4) HBs with lipids emerged. From a dynamic perspective, lifetimes reinforce the influence of the environment on the persistence of interactions. In vacuum, intramolecular HBs exhibited lifetimes of 251.9 ps, but in water this increased to 607.2 ps (+141%) due to conformational reorganization promoted by solvation. The membrane impact was even more significant: in the DOPC–water system, intramolecular lifetimes reached 2010 ps, corresponding to a 231% increase relative to water. For peptide–solvent interactions, an opposite trend was observed: in water, HBs lasted only 9.6 ps, but in the presence of the bilayer their persistence increased to 50 ps (+421%), reflecting the reduced mobility of water near the lipid interface.

Table 3
Average number of hydrogen bonds (#HB), lifetimes (ps), and free energy of bond rupture (ΔG, kJ/mol) for NP-3a in three simulated environments: vacuum, water, and DOPC-water. Values are reported for peptide-peptide, peptide-water, and peptide-DOPC interactions. HBs were defined using a distance cutoff of $r \leq 0.35$ nm (donor-acceptor) and an angle cutoff $\leq 30°$ (hydrogen-donor-acceptor). Lifetimes and ΔG values were calculated following the theoretical framework of Luzar and Chandler (Luzar, 2000; Luzar and Chandler, 1996) and van der Spoel et al (Van Der Spoel et al., 2006)., which account for intermittent bond dynamics and free energy estimation from HBs correlation functions. Here, peptide-peptide interaction refers to intramolecular interactions within the single NP-3a molecule.

	# HB		
	In-vacuum	In-water	In-DOPC
Peptide-Peptide	23 ± 2	6 ± 2	4 ± 2
Peptide-Water	–	122 ± 6	110 ± 7
Peptide-DOPC	–	–	12 ± 4
	HB's Lifetime (ps)		
	In-vacuum	In-vacuum	In-vacuum
Peptide-Peptide	251.9	607.2	2010.0
Peptide-Water	–	9.6	50.0
Peptide-DOPC	–	–	2950.0
	ΔG (kJ/mol)		
	In-vacuum	In-vacuum	In-vacuum
Peptide-Peptide	18.2	20.4	23.4
Peptide-Water	–	10.1	14.2
Peptide-DOPC	–	–	24.3

Direct peptide-DOPC HBs showed the highest stability, with 2950 ps, essentially remaining fixed throughout the simulation. Free energy values (ΔG) followed similar trends. Intramolecular HBs exhibited ΔG of 18.2 kJ/mol in vacuum, rising to 20.4 kJ/mol in solution (+12%) and reaching 23.4 kJ/mol in the presence of the bilayer (+15% relative to water). For peptide-water interactions, stability was lower, with ΔG of 10.1 kJ/mol in water, but increased to 14.2 kJ/mol (+41%) in the lipid environment, corroborating the enhanced persistence observed in lifetimes. Finally, peptide-DOPC bonds displayed ΔG of 24.3 kJ/mol, the highest value overall, confirming their highly stable character. These results demonstrate that the environment modulates both the number and stability of NP-3a HBs. Vacuum favors internal compaction, whereas water disrupts the intramolecular network in favor of transient external contacts. The bilayer not only restores part of the internal HBs but also significantly stabilizes intermolecular contacts, particularly those with the polar groups of DOPC. Thus, the membrane confers on NP-3a a regime of highly stable anchoring, supported by a small number of specific interactions of long duration and high energy, consistent with its biological role in recognizing and modulating the lipid interface.

The NP-3a peptide consists of 33 amino acids with the primary sequence NH_2-GICACRRRFCPNSERFSGYCRVNGARYVRCCSRR-COOH, flanked by an N-terminal amine (–NH_2) and a C-terminal carboxyl group (–COOH). In the present analysis, amino acids are numbered sequentially from the N-terminus. Within this framework, Ser-3, Cys-5, Cys-6, Arg-6, Arg-7, Arg-8, Arg-9, and Tyr-2 are identified as residues of interest in the peptide. This numbering refers to their position within the peptide chain and facilitates the decomposition of interactions by residue, allowing quantification of their individual contributions to HBs with solvent and DOPC lipids (see Table 4). The highlighted residues represent sites where HBs was not only detected but also characterized by high stability, long lifetime, or elevated free energy of interaction, underscoring their disproportionate importance relative to their frequency in the sequence. The residue-level decomposition of HBs interactions revealed that stabilization of NP-3a at the DOPC membrane interface is disproportionately mediated by a small subset of amino acids. Despite accounting for less than one quarter of the peptide's sequence (~23.5%), these residues concentrate the majority of stable and long-lived contacts with the lipid bilayer. Among them, the arginine triad (Arg-6, Arg-7, Arg-8, and Arg-9) emerged as the dominant contributors, forming between 1.5 – 3.2 HBs on average, with lifetimes ranging from ~1.9 to ~3.4 ns and free energies consistently above 23 kJ/mol. These values indicate that the cationic guanidinium groups of arginine residues not only initiate recognition of negatively charged phosphate groups but also sustain highly persistent electrostatic anchoring at the lipid interface. In comparison, serine (Ser-3) played a complementary role. Although the average number of HBs formed by serine (0.7 ± 0.7 HBs) was lower than that of arginine, the corresponding lifetime (2806 ps; ~2.8 ns) and free energy (24.2 kJ/mol) were within the same magnitude as the arginine residues.

Table 4
Residue-level decomposition of hydrogen bonding interactions for NP-3a at the DOPC bilayer interface. Reported values include the average HBs lifetime (ps), free energy of HB rupture (ΔG, kJ/mol), and average number of hydrogen bonds (#HBs) for each terminal residue of the NP-3a. Data highlight the disproportionate contribution of selected residues, particularly arginine (Arg-6 to Arg-9), serine (Ser-3), and cysteines (Cys-5 and Cys-6), to peptide anchoring and stabilization at the membrane surface. Lifetimes and ΔG values were calculated following the theoretical framework of Luzar and Chandler (Luzar, 2000; Luzar and Chandler, 1996) and van der Spoel et al (Van Der Spoel et al., 2006)., which account for intermittent bond dynamics and free energy estimation from HBs correlation functions.

NP-3a's Residue	#HBs	HB-lifetime (ps)	ΔG (kJ/mol)
Arg-6	1.5 ± 0.8	2696.0	24.1
Tyr-2	0.3 ± 0.5	599.3	20.4
Arg-7	2.5 ± 1.6	3365.9	24.7
Cys-5	0.3 ± 0.5	11,205.7	27.6
Cys-6	0.4 ± 0.5	1248.0	22.2
Ser-3	0.7 ± 0.7	2806.1	24.2
Arg-8	2.5 ± 1.3	1853.9	23.2
Arg-9	3.2 ± 1.1	2095.7	23.5

These results suggests that the hydroxyl group of serine, while less frequently engaged, establishes stable polar contacts once positioned near the membrane. Such interactions are likely to act cooperatively with arginine-mediated electrostatics, providing additional stabilization by bridging water molecules and lipid headgroups in the interfacial region. A distinct behavior was observed for cysteines (Cys-5 and Cys-6). While both residues exhibited relatively low average HBs counts (0.3 ± 0.5 and 0.4 ± 0.5 HBs, respectively), their interaction lifetimes diverged sharply. Cys-6 displayed moderate persistence (~1.3 ns, ΔG = 22.2 kJ/mol), whereas Cys-5 formed contacts with extraordinarily long duration, exceeding ~11,206 ps (~11 ns) and reaching the highest free energy value recorded in the dataset (27.6 kJ/mol). This result highlights a stabilizing role for Cys-5 that differs from the electrostatic anchoring of arginine or the bridging capacity of serine. Instead, it functions as a structural anchor, reinforcing the peptide's residence time at the interface through exceptionally stable HBs. Taken together, these findings delineate a multifactorial anchoring mechanism for NP-3a. The arginine residues provide dominant electrostatic recognition and orientation toward the bilayer, serine contributes flexible but stable polar contacts that reinforce the interfacial positioning, and cysteines (particularly Cys-5) act as structural stabilizers through unusually persistent interactions. This spatial and functional organization supports a model in which NP-3a achieves stable surface localization at the DOPC bilayer without penetrating deeply into the hydrophobic core, a mechanism consistent with selective antimicrobial activity that perturbs the membrane interface while preserving overall bilayer integrity. These results reveal a two-step interfacial mechanism: (i) electrostatic capture by clustered arginine residues, followed by (ii) structural locking through long-lived cysteine interactions and limited hydrophobic burial. Rather than disrupting membrane integrity directly, NP-3a behaves as a surface "electrostatic clamp", consistent with a non-lytic mode of action that could initiate later oligomerization or cooperative pore formation with other defensins.

The persistence of intramolecular HBs following membrane association suggests partial stabilization of β-sheet structural elements at the lipid interface, although the peptide remains dynamically heterogeneous. Thus, the set of results related to HBs indicates a dynamic balance between structural preservation of the peptide at the membrane interface and flexibility of certain solvent-exposed regions. This interpretation supports the view that the peptide's anchoring behavior is associated with localized structural stabilization rather than global conformational collapse.

3.3. Peptide anchoring and membrane association

It is important to emphasize that the DOPC bilayer employed here represents a eukaryotic-like membrane model rather than a bacterial membrane mimic. The observed surface localization of NP-3a should therefore not be interpreted as evidence of weak antimicrobial activity, but rather as an indication of limited insertion into membranes lacking anionic lipids. In this sense, the persistent interfacial anchoring without deep penetration observed in DOPC provides molecular insight into the selectivity of NP-3a, which is known experimentally to preferentially disrupt bacterial membranes while sparing eukaryotic cells. The spatial organization of NP-3a relative to the DOPC bilayer provides critical insight into its mechanism of membrane interaction. Density profiles of lipids, water, ions, and peptide along the bilayer normal (see Fig. 2) reveal a clear segregation of components: water dominates the bulk phases, lipids define the interfacial boundaries with the characteristic headgroup peaks, and the hydrophobic core is devoid of solvent. NP-3a is localized precisely at the interfacial zone, overlapping with the polar headgroups of DOPC but avoiding penetration into the hydrophobic

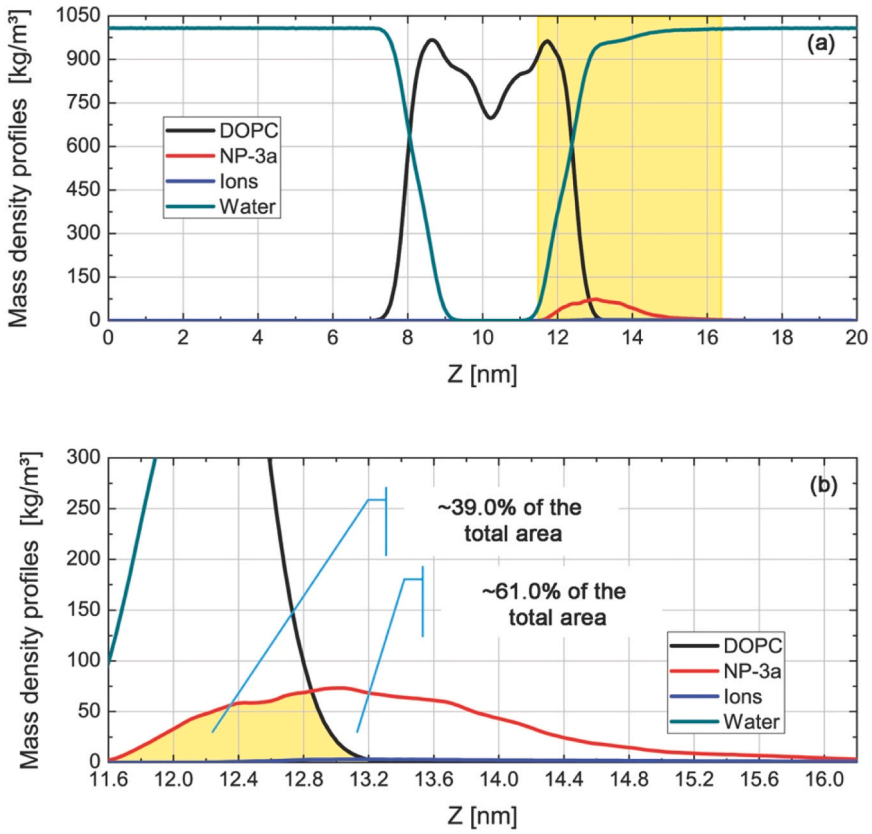

Fig. 2. (a) Mass density profiles of NP-3a, DOPC lipids, water, and ions along the bilayer normal (z-axis), and (b) highlight for NP-3a mass density profile and mass percentage penetration. Water (blue) dominates the bulk phases and is excluded from the hydrophobic core, while DOPC (green) exhibits the characteristic headgroup peaks flanking the bilayer interior. Ion density (red) is restricted to the aqueous phase, with mild accumulation near the interface. The peptide profile (black) overlaps with the lipid headgroup region, demonstrating that NP-3a localizes at the interfacial zone rather than penetrating the hydrophobic core. The shaded region highlights the anchoring zone where peptide density coincides with DOPC headgroups, consistent with selective surface adsorption.

interior (~39% penetrate under the conditions investigated). This distribution establishes that the peptide is stabilized at the membrane–-water interface, consistent with a selective adsorption rather than a disruptive insertion mechanism. The temporal evolution of this process is illustrated by simulation snapshots spanning 5–100 ns (see Fig. 3). At the earliest stages, NP-3a remains partially solvated and only associated with the bilayer surface. As the trajectory progresses, side chains rich in arginine and serine gradually engage with the lipid headgroups, driving reorientation of the peptide and promoting stable anchoring parallel to the membrane plane.

By 100 ns, the peptide achieves persistent contact with the interfacial region, supported by multiple residues, while remaining excluded from the hydrophobic core. This dynamic progression from initial recognition to stable adsorption underscores the role of specific residues in mediating membrane affinity. The energetic profile of NP-3a binding aligns closely with these structural observations. Electrostatic interactions between the peptide and DOPC were substantial, vastly outweighing peptide–ion interactions and highlighting the phosphate headgroups as the principal electrostatic partners. Van der Waals contacts provided an additional stabilizing contribution, particularly as hydrophobic side chains approached the interfacial region. The combination of strong long-range electrostatics and moderate van der Waals interactions explains the preference for surface anchoring (under the conditions investigated): recognition and retention at the headgroup region are favored, whereas deep insertion into the hydrophobic core is not energetically supported. HBs analyses further consolidate this picture, NP-3a formed, on average, ~12 HBs with DOPC headgroups, characterized by exceptionally long lifetimes (between 1 and 3 ns) and high free energies of rupture (~24 kJ/mol). These values far exceeded those observed for peptide–solvent interactions, confirming the selective stabilization conferred by lipid headgroups. Thus, Figs. 2 and 3, when integrated with energetic and HBs data, portray a coherent mechanism: NP-3a anchors at the DOPC interface through a synergistic network of cationic and polar residues, achieving durable surface localization while avoiding disruptive penetration into the bilayer core (under the conditions investigated). This mechanism is consistent with antimicrobial selectivity, enabling membrane modulation without compromising overall bilayer integrity.

3.4. *Peptide solvent-accessible surface and Einstein's diffusion coefficient*

The solvent-accessible surface area (SASA) and the Einstein diffusion coefficient provide complementary descriptors of NP-3a dynamics across different environments. In aqueous solution, the peptide exhibits a large SASA, reflecting extensive solvent exposure and conformational flexibility, consistent with its transient HBs network. At the same time, the diffusion coefficient indicates higher mobility in water, characteristic of unrestricted translational motion in a bulk polar environment. In contrast, when associated with a DOPC bilayer, NP-3a displays a reduced SASA, indicative of partial shielding of residues by lipid headgroups and stabilization at the membrane interface. The diffusion coefficient decreases markedly under these conditions, confirming that peptide mobility is restricted by electrostatic and HBs interactions with the bilayer. Together, these results demonstrate a clear transition from a dynamic, solvent-exposed peptide in water to a structurally restrained and locally immobilized state upon anchoring to the lipid membrane.

The quantitative analysis confirms that NP-3a presents a solvent-accessible surface area (SASA) of approximately 44.7 ± 2.8 nm^2 when

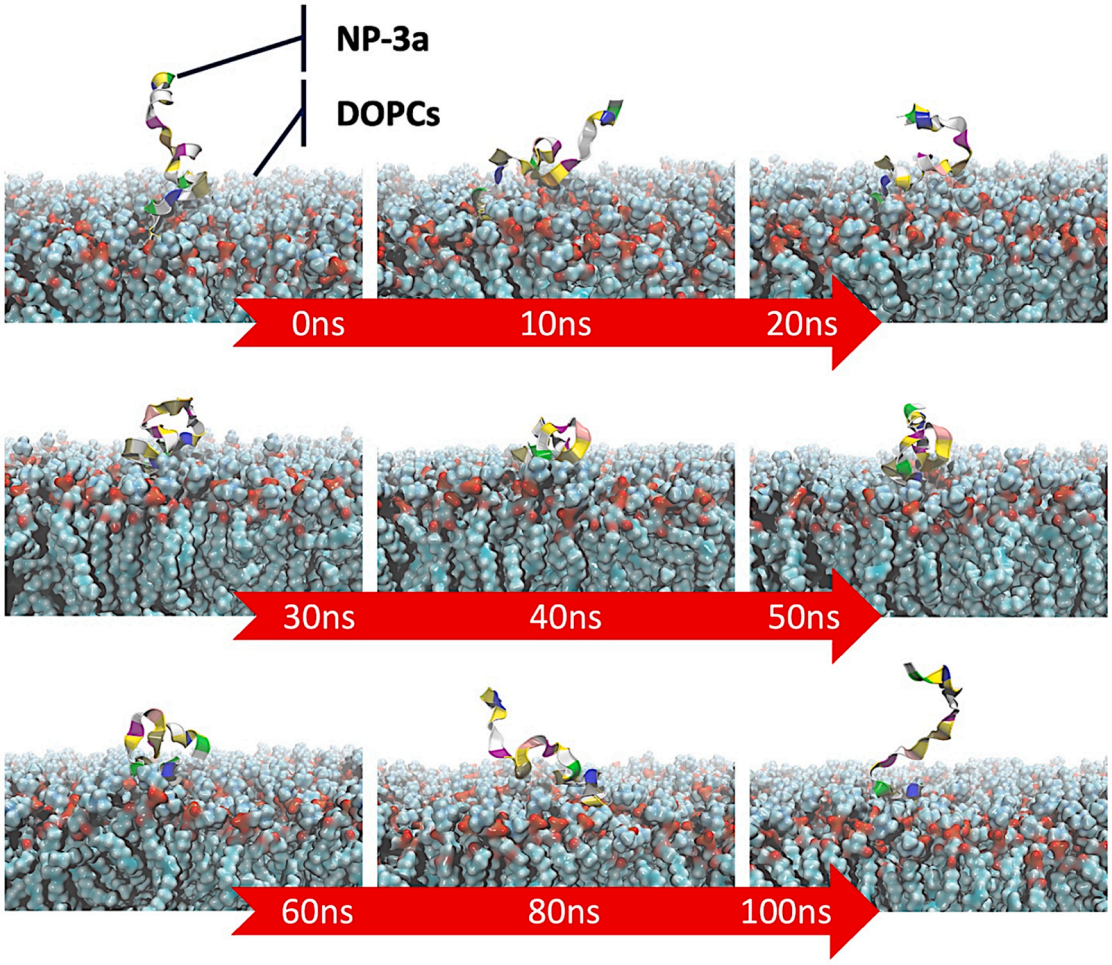

Fig. 3. Temporal sequence of NP-3a interacting with the DOPC bilayer at 0, 10, 20, 30, 40, 50, 60, 80, and 100 ns (production stage of the MD-simulation). The peptide is shown in ribbon, lipid headgroups and tails in red and blue, respectively, and ions and water molecules are omitted for clarity. The sequence highlights that NP-3a remains associated with the interfacial region throughout, achieving stable anchoring without insertion into the bilayer hydrophobic core.

in aqueous solution, consistent with antimicrobial peptides of comparable size. This large exposure to water reflects its conformational flexibility and transient HBs with solvent molecules. Upon interaction with the DOPC bilayer, SASA values decrease by ~11% (40.0 $\pm$ 3.9 nm^2), indicating that a significant fraction of polar and cationic residues becomes shielded by the lipid headgroups during anchoring. This reduction is in agreement with the density profiles and residue-level HBs analysis, which demonstrated that arginine and serine residues preferentially establish contacts with the interfacial region rather than remaining fully exposed to the solvent. A similar trend is observed for the Einstein diffusion coefficient (MSD), which was calculated from the linear regime of the mean squared displacement extracted over the first 10 ns of the production trajectory. In bulk water, NP-3a displays translational diffusivity on the order of $(1.6 \pm 0.1) \times 10^{-6}$ cm^2/s, comparable to typical peptides in water solution. Upon adsorption at the DOPC bilayer, diffusivity decreases to $(1.4 \pm 0.1) \times 10^{-6}$ cm^2/s, reflecting restricted lateral and translational motion imposed by electrostatic anchoring and long-lived HBs with lipid headgroups. This decrease in diffusion, combined with reduced SASA, underscores the shift from a highly dynamic peptide in solution to a structurally stabilized and locally immobilized state at the membrane interface, consistent with its antimicrobial mechanism of selective surface localization.

3.5. Membrane thickness and peptide-induced deformation

The structural properties of lipid bilayers, such as membrane thickness, play a fundamental role in determining their stability and their ability to interact with peptides and proteins. Variations in bilayer thickness can directly reflect perturbations induced by external molecules, particularly antimicrobial peptides that associate with the membrane interface. In order to quantitatively assess these structural changes, the SuAVE software (Santos et al., 2020) was employed to calculate the average thickness of the DOPC bilayer under two conditions: in the absence of peptide and in the presence of NP-3a. This analysis allows for the direct comparison of baseline bilayer properties with those perturbed by peptide anchoring. In the control system without NP-3a, the DOPC bilayer is expected to maintain a symmetric structure with a uniform thickness characteristic of DOPC membranes. The introduction of NP-3a, however, promotes localized deformations due to its anchoring at the interfacial region. By calculating thickness maps and extracting average values across the bilayer plane, it becomes possible to quantify not only global changes in bilayer thickness but also the spatially localized distortions arising from direct peptide–lipid interactions. These metrics complement the energetic and HBs analyses previously described, offering a structural perspective on peptide-induced membrane perturbation. Fig. 4 illustrates these effects by contrasting the bilayer thickness distributions in the absence and presence of NP-3a. While the control bilayer exhibits a homogeneous profile, the peptide-bound system reveals regions of reduced thickness that coincide with the peptide anchoring site. These deformations are consistent with the role of cationic and polar residues in perturbing lipid headgroups and stabilizing peptide localization at the membrane

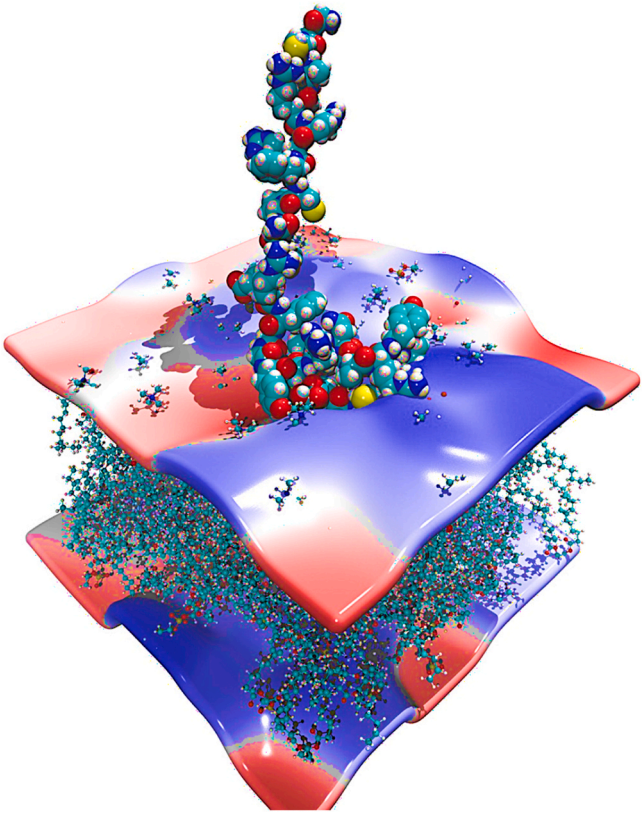

Fig. 4. NP-3a anchored at the interface of the lipid membrane. Surface map obtained with SuAVE. The MD-configuration highlights localized thinning of the bilayer at the peptide binding site, consistent with interfacial perturbation induced by anchoring.

surface. Such findings bridge structural and energetic perspectives, reinforcing the conclusion that NP-3a stabilizes at the interface without penetrating deeply into the bilayer core.

The average thickness of the DOPC bilayer in the absence of peptide was found to be close to 4.21 ± 0.07 nm, a value consistent with experimental and computational reports for lipid membranes (Alves et al., 2020). This uniform thickness reflects the structural symmetry of the bilayer and the absence of external perturbations. When NP-3a was introduced, the average thickness increased by approximately 3%, leading to values in the range of 4.32 ± 0.04 nm. Thickness maps revealed that this reduction was not uniform across the bilayer plane but rather localized in the region underlying the peptide anchoring site, where side chains such as arginine and serine interact strongly with lipid headgroups. The observed increase in thickness therefore represents a structural manifestation of peptide anchoring, reinforcing the conclusion that NP-3a perturbs the bilayer surface selectively under the conditions investigated. Such interfacial thinning may facilitate membrane permeabilization in a controlled, non-lytic manner, consistent with NP-3a's role as a selective antimicrobial peptide.

4. Conclusions

The simulations support a model in which NP-3a operates through interfacial adsorption as a precursor to cooperative mechanisms such as membrane thinning, clustering of anionic lipids, or defensin oligomerization (processes widely implicated in AMP activity but rarely resolved at atomistic resolution for rabbit defensins). In this context, one of the central strengths of the present study lies in the integration of structural, energetic, HBs, dynamical, and membrane-thickness analyses within a single coherent atomistic framework. Thus, this work provides atomistic evidence of how the antimicrobial peptide NP-3a adapts structurally and energetically to distinct environments through a controlled hierarchical simulation strategy (vacuum, aqueous solution, and membrane interface), allowing intrinsic peptide stabilization to be disentangled from solvent- and membrane-induced effects.

In vacuum, the peptide retains a compact structure stabilized by intramolecular disulfide bonds and extensive HBs, with an average of ~23 intramolecular HBs and strong Coulomb stabilization (−2779.7 kJ/mol), representing its maximally compact reference state. When solvated in water, this compactness is lost, giving rise to a highly dynamic state characterized by a sharp reduction in intramolecular HBs (~74% decrease) and the formation of numerous, short-lived interactions with solvent molecules (~122 HBs, average lifetime ~9.6 ps). These results quantitatively highlight the conformational flexibility of NP-3a and its ability to reorganize in polar environments, demonstrating that solvent screening significantly redistributes electrostatic and van der Waals contributions. In the presence of a DOPC bilayer, NP-3a achieves stable anchoring at the membrane interface without penetrating the hydrophobic core. This behavior is underpinned by strong electrostatic interactions with lipid headgroups (−842 kJ/mol) and long-lived HBs (average lifetime ~3 ns; ΔG ~24.3 kJ/mol), which greatly exceed the persistence of peptide-solvent contacts. Notably, anchoring is not driven by the quantity of interactions but by their energetic and temporal stability, as ~12 peptide-DOPC's HBs establish a persistent interfacial state between NP-3a and DOPCs. The residue-level decomposition identified Arg-7, Arg-8, and Arg-9 as key contributors to interfacial recognition, supported by Ser-3 and Cys-5, whose unusually long-lived contacts act as structural anchors. This residue-specific quantitative analysis represents a significant mechanistic contribution of the study, revealing a multifactorial binding mechanism in which cationic residues provide electrostatic attraction, polar residues stabilize the interfacial network, and cysteines reinforce anchoring through persistent interactions.

Structural and dynamical metrics further consolidate this mechanistic interpretation. The solvent-accessible surface area decreases by approximately 11% upon membrane association (from ~44.7 nm^2 in water to ~40.0 nm^2 at the interface), while the diffusion coefficient is reduced from $(1.6 \pm 0.1) \times 10^{-6}$ cm^2/s in water, reflecting restricted mobility and local immobilization at the membrane surface. In parallel, membrane-thickness analysis revealed localized perturbation (~3% variation) at the anchoring site, providing structural evidence of interfacial modulation without catastrophic bilayer disruption. Together, these convergent energetic, structural, and dynamical signatures establish a robust and internally consistent description of NP-3a surface stabilization. These findings, under the MD-conditions simulated, validate NP-3a's experimentally reported broad-spectrum antimicrobial activity and its preference for membrane permeabilization through surface association rather than deep insertion. The consistency between simulations and experimental evidence for rabbit defensins (NP-1 to NP-5) underscores the functional relevance of this mechanism. The use of a DOPC bilayer allowed us to probe NP-3a behavior at a eukaryotic-like membrane interface, revealing stable surface anchoring without deep insertion within the simulated timescale. This controlled reference system enabled clear identification of electrostatic capture, HBs persistence, and residue-specific stabilization as central determinants of anchoring. This behavior is consistent with antimicrobial selectivity and supports the notion that stronger insertion and permeabilization are expected in anionic bacterial membranes.

To appropriately frame these results, it is important to recognize the defined scope of the present model. The simulations were conducted for a single NP-3a molecule interacting with a simplified *zwitterionic* DOPC bilayer and within the nanosecond timescale accessible to atomistic molecular dynamics. While this controlled framework enables precise characterization of interfacial anchoring mechanisms and energetic determinants, it does not explicitly address cooperative peptide assembly or the full compositional diversity of bacterial membranes. These considerations define the boundaries of the present study and indicate natural directions for future extensions, without affecting the robustness

of the mechanistic insights reported in this work.

CRediT authorship contribution statement

Karinna Mendanha: Writing – review & editing, Writing – original draft, Visualization, Validation, Methodology, Investigation, Formal analysis, Data curation. **Aquino Ana Clara D.:** Writing – review & editing, Writing – original draft, Visualization, Validation, Methodology, Investigation, Formal analysis, Data curation. **Guilherme Colherinhas:** Writing – review & editing, Writing – original draft, Visualization, Validation, Supervision, Resources, Project administration, Methodology, Investigation, Funding acquisition, Formal analysis, Data curation, Conceptualization. **Georg Herbert de C.:** Writing – review & editing, Writing – original draft, Visualization, Validation, Supervision, Methodology, Investigation, Formal analysis, Data curation.

Declaration of Competing Interest

The authors declare that they have no known competing financial interests or personal relationships that could have appeared to influence the work reported in this paper.

Acknowledgements

This work was supported by research grants from the National Council for Scientific and Technological Development (CNPq), the Coordination for the Improvement of Higher Education Personnel (CAPES), and the Goiás Research Foundation (FAPEG). The authors gratefully acknowledge the use of the Multiuser Laboratory for Scientific Computing of the Institute of Physics – Federal University of Goiás (UFG).

References

Abraham, M., Alekseenko, A., Bergh, C., Blau, C., Briand, E., Doijade, M., Fleischmann, S., Gapsys, V., Garg, G., Gorelov, S., Gouaillardet, G., Gray, A., Irrgang, M.E., Jalalypour, F., Jordan, J., Junghans, C., Kanduri, P., Keller, S., Kutzner, C., Lemkul, J.A., Lundborg, M., Merz, P., Miletić, V., Morozov, D., Páll, S., Schulz, R., Shirts, M., Shvetsov, A., Soproni, B., D. van der, Spoel, Turner, P., Uphoff, C., Villa, A., Wingbermühle, S., Zhmurov, A., Bauer, P., Hess, B., Lindahl, E. G.R.O.M.A.C.S., 2023. Manual 2023. https://doi.org/10.5281/ZENODO.7588711.

Abraham, M.J., Murtola, T., Schulz, R., Páll, S., Smith, J.C., Hess, B., Lindah, E., 2015. Gromacs: high performance molecular simulations through multi-level parallelism from laptops to supercomputers, 19–25 SoftwareX *1–2*. https://doi.org/10.1016/j.softx.2015.06.001.

Alves, E.D., Colherinhas, G., Mendanha, S.A., 2020. Assessing the DOPC-cholesterol interactions and their influence on fullerene C60 partitioning in lipid bilayers. J. Mol. Liq. 315, 113698. https://doi.org/10.1016/j.molliq.2020.113698.

Aunpad, R., Thitirungreangchai, T., 2025. Advancing antimicrobial peptides: overcoming challenges in the era of bacterial resistance. Biochimie. Elsevier B.V. https://doi.org/10.1016/j.biochi.2025.07.019.

Best, R.B., Zhu, X., Shim, J., Lopes, P.E.M., Mittal, J., Feig, M., MacKerell, A.D., 2012. Optimization of the additive CHARMM all-atom protein force field targeting improved sampling of the backbone φ, ψ and side-chain X1 and X2 dihedral angles. J. Chem. Theory Comput. 8 (9), 3257–3273. https://doi.org/10.1021/ct300400x.

Brooks, B.R., Brooks, C.L., Mackerell, A.D., Nilsson, L., Petrella, R.J., Roux, B., Won, Y., Archontis, G., Bartels, C., Boresch, S., Caflisch, A., Caves, L., Cui, Q., Dinner, A.R., Feig, M., Fischer, S., Gao, J., Hodoscek, M., Im, W., Kuczera, K., Lazaridis, T., Ma, J., Ovchinnikov, V., Paci, E., Pastor, R.W., Post, C.B., Pu, J.Z., Schaefer, M., Tidor, B., Venable, R.M., Woodcock, H.L., Wu, X., Yang, W., York, D.M., Karplus, M., 2009. CHARMM: the biomolecular simulation program. J. Comput. Chem. 30 (10), 1545–1614. https://doi.org/10.1002/jcc.21287.

Bussi, G., Donadio, D., Parrinello, M., 2007. Canonical sampling through velocity rescaling. J. Chem. Phys. 126 (1), 014101. https://doi.org/10.1063/1.2408420.

Castelletto, V., Barnes, R.H., Karatzas, K.A., Edwards-Gayle, C.J.C., Greco, F., Hamley, I. W., Rambo, R., Seitsonen, J., Ruokolainen, J., 2018. Arginine-containing surfactant-like peptides: interaction with lipid membranes and antimicrobial activity. Biomacromolecules 19 (7), 2782–2794. https://doi.org/10.1021/acs.biomac.8b00391.

Castelletto, V., Seitsonen, J., de Mello, L.R., Hamley, I.W., 2024. Interaction of arginine-rich surfactant-like peptide nanotubes with liposomes. Biomacromolecules 25 (11), 7410–7420. https://doi.org/10.1021/acs.biomac.4c01072.

Coelho, E., de Andrade, D.X., Colherinhas, G., 2023. Exploring fullerenol-C60(OH)24 interactions with lipid bilayers: molecular dynamics study of agglomeration and surface deposition. J. Mol. Liq. 391, 123205. https://doi.org/10.1016/j.molliq.2023.123205.

Colherinhas, G., 2021a. Update of CHARMM36's atomic charges for aromatic amino acids in water solution simulations and spectroscopy analysis via sequential molecular dynamics and DFT calculations. J. Mol. Liq. 321, 114739. https://doi.org/10.1016/j.molliq.2020.114739.

Colherinhas, G., 2021b. Updating atomic charge parameters of aliphatic amino acids: a quest to improve the performance of molecular modelingviasequential molecular dynamics and DFT-GIAO NMR calculations. Phys. Chem. Chem. Phys. 23 (14), 8413–8425. https://doi.org/10.1039/d1cp00183c.

Darden, T., York, D., Pedersen, L., 1993. Particle mesh ewald: an N·log(N) method for ewald sums in large systems. J. Chem. Phys. 98 (12), 10089–10092. https://doi.org/10.1063/1.464397.

Du, Z., Fan, B., Dai, Q., Wang, L., Guo, J., Ye, Z., Cui, N., Chen, J., Tan, K., Li, R., Tang, W., March 1, 2022. Supramolecular peptide nanostructures: self-assembly and biomedical applications. Giant. Elsevier B.V. https://doi.org/10.1016/j.giant.2021.100082.

Edwards-Gayle, C.J.C., Hamley, I.W., 2017. Self-assembly of bioactive peptides, peptide conjugates, and peptide mimetic materials. Organic and Biomolecular Chemistry. Royal Society of Chemistry, pp. 5867–5876. https://doi.org/10.1039/c7ob01092c.

Hess, B., Bekker, H., Berendsen, H.J.C., Fraaije, J.G.E.M., 1997. LINCS: a linear constraint solver for molecular simulations. J. Comput. Chem. 18 (12), 1463–1472. https://doi.org/10.1002/(SICI)1096-987X(199709)18:12<1463::AID-JCC4>3.0.CO;2-H.

Hristova, K., Selsted, M.E., White, S.H., 1997. Critical role of lipid composition in membrane permeabilization by rabbit neutrophil defensins. J. Biol. Chem. 272 (39), 24224–24233. https://doi.org/10.1074/jbc.272.39.24224.

Huan, Y., Kong, Q., Mou, H., Yi, H., October 16, 2020. Antimicrobial peptides: classification, design, application and research progress in multiple fields. Frontiers in Microbiology. Frontiers Media S.A. https://doi.org/10.3389/fmicb.2020.582779.

Humphrey, W., Dalke, A., Schulten, K., 1996. VMD: visual molecular dynamics. J. Mol. Graph. 14 (1), 33–38. https://doi.org/10.1016/0263-7855(96)00018-5.

Hwang, D., Kim, H.J., 2024. Increased antimicrobial resistance of acid-adapted pathogenic Escherichia coli, and transcriptomic analysis of polymyxin-resistant strain. Microb. Pathog. 196. https://doi.org/10.1016/j.micpath.2024.106974.

Jorgensen, W.L., Chandrasekhar, J., Madura, J.D., Impey, R.W., Klein, M.L., 1983. Comparison of simple potential functions for simulating liquid water. J. Chem. Phys. 79 (2), 926–935. https://doi.org/10.1063/1.445869.

Jorgensen, W.L., Maxwell, D.S., Tirado-Rives, J., 1996. Development and testing of the OPLS all-atom force field on conformational energetics and properties of organic liquids. J. Am. Chem. Soc. 118 (45), 11225–11236. https://doi.org/10.1021/JA9621760/SUPPL_FILE/JA11225.PDF.

Li, X., Ding, Y., Xue, J., Fu, Y., Yan, F., Song, N., Hu, H., Cong, W., Lu, Z., Li, Y., 2025. Peptide double-stapling and arginine N-glycosylation triggered the development of therapeutic antimicrobial peptides capable of killing drug-resistant bacteria in mice. J. Med. Chem. 68 (4), 4511–4526. https://doi.org/10.1021/acs.jmedchem.4c02564.

Liu, L., Cui, X., Zhang, H., Yao, J., Li, L., Cai, Y., 2025. Optimized strategies for designing antimicrobial peptides targeting multidrug-resistant gram-negative bacteria. Biomed. Pharmacother. 189. https://doi.org/10.1016/j.biopha.2025.118264.

Luo, X., Chen, H., Song, Y., Qin, Z., Xu, L., He, N., Tan, Y., Dessie, W., February 1, 2023. Advancements, challenges and future perspectives on peptide-based drugs: focus on antimicrobial peptides. European Journal of Pharmaceutical Sciences. Elsevier B.V. https://doi.org/10.1016/j.ejps.2022.106363.

Luzar, A., 2000. Resolving the hydrogen bond dynamics conundrum. J. Chem. Phys. 113 (23), 10663–10675. https://doi.org/10.1063/1.1320826.

Luzar, A., Chandler, D., 1996. Hydrogen-bond kinetics in liquid water. Nature 379 (6560), 55–57. https://doi.org/10.1038/379055a0.

Ma, X., Mao, R., Hao, Y., Li, Y., Li, X., Teng, D., Yang, N., Wang, J., 2025. Self-assembly of antimicrobial peptide nanofibers enhances enzymatic stability for dual-mode capture and killing of multidrug-resistant clinical isolates. Chem. Eng. J. 519. https://doi.org/10.1016/j.cej.2025.165462.

Malaspina, T., Colherinhas, G., De Oliveira Outi, F., Fileti, E.E., 2017. Assessing the interaction between surfactant-like peptides and lipid membranes. RSC Adv. 7 (57), 35973–35981. https://doi.org/10.1039/c7ra04537a.

Mendanha, K., Colherinhas, G., 2024. Exploring how system dimensions and periodic boundary conditions influence the molecular dynamics simulation of A $_6$ H peptide self-assembly nanostructures. J. Phys. Chem. B 128 (28), 6853–6865. https://doi.org/10.1021/acs.jpcb.4c03043.

Oliveira, L.B.A., Colherinhas, G., 2020. Can CHARMM36 atomic charges described correctly the interaction between amino acid and water molecules by molecular dynamics simulations? J. Mol. Liq. 317, 113919. https://doi.org/10.1016/j.molliq.2020.113919.

Osei, K.J., Wereko Brobbey, D. youngster, Tetteh, J., Laryea, M.K., Darko, G., Borquaye, L.S., 2025. Peptide extract from hexaplex trunculus: a promising antimicrobial agent with inhibitory effects on quorum sensing and biofilm formation. Pharmacol. Res. Nat. Prod. 8. https://doi.org/10.1016/j.prenap.2025.100315.

Parrinello, M., Rahman, A., 1981. Polymorphic transitions in single crystals: a new molecular dynamics method. J. Appl. Phys. 52 (12), 7182–7190. https://doi.org/10.1063/1.328693.

Peng, X., Luo, Y., Xu, T., Chen, Z., Chen, P., Hu, C., Liu, S., 2025. Antibiotic-conjugated antimicrobial peptides for enhanced bacterial inhibition. RSC Adv. 15 (25), 19751–19761. https://doi.org/10.1039/d5ra02932e.

Santos, D.E.S., Pontes, F.J.S., Lins, R.D., Coutinho, K., Soares, T.A., 2020. SuAVE: a tool for analyzing curvature-dependent properties in chemical interfaces. J. Chem. Inf. Model. 60 (2), 473–484. https://doi.org/10.1021/acs.jcim.9b00569.

Schmidtchen, A., Malmsten, M., 2013. Peptide Interactions with Bacterial Lipopolysaccharides. Curr. Opin. Colloid Interface Sci. 381–392. https://doi.org/10.1016/j.cocis.2013.06.003.

Schrödinger. The PyMOL Molecular Graphics System. LLC 2015. ⟨https://www.pymol.org/#page-top⟩ (accessed 2025-02-09).

Van Der Spoel, D., Van Maaren, P.J., Larsson, P., Tîmneanu, N., 2006. Thermodynamics of hydrogen bonding in hydrophilic and hydrophobic media. J. Phys. Chem. B 110 (9), 4393–4398. https://doi.org/10.1021/jp0572535.

Yang, Q., Hu, Z., Jiang, H., Wang, J., Han, H., Shi, W., Qian, H., 2025. Recent advances, strategies, and future perspectives of peptide-based drugs in clinical applications. Chinese Journal of Natural Medicines. China Pharmaceutical University January, pp. 31–42. https://doi.org/10.1016/S1875-5364(25)60800-4.

Yu, W., Guo, X., Li, X., Wei, Y., Lyu, Y., Zhang, L., Wang, J., Shan, A., 2024. Novel multidomain peptide self-assembly biomaterials based on bola structure and terminal anchoring: nanotechnology meets antimicrobial therapy. Mater. Today Bio 28. https://doi.org/10.1016/j.mtbio.2024.101183.

Yuan, J.X., Gao, Y.J., Hua, R., Wei, T.C., Xu, G.Y., Zhou, J., Zhang, K., Li, Y.T., Feng, J.Q., Lai, W.J., Wang, L., Chen, X., 2025. Antimicrobial effects of fibrous unit in modular self-assembling peptides. Nano Today 65. https://doi.org/10.1016/j.nantod.2025.102860.